

New prototype scintillator detector for the Tibet AS γ Experiment

Y. Zhang,^a Q.-B. Gou,^a H. Cai,^{b,a} T.-L. Chen,^c Danzengluobu,^c C.-F. Feng,^d Y.-L. Feng,^{a,e} Z.-Y. Feng,^a Q. Gao,^c X.-J. Gao,^a Y.-Q. Guo,^a Y.-Y. Guo,^{a,e} Y.-Y. Hou,^a H.-B. Hu,^{a,e} C. Jin,^{a,e} H.-J. Li,^c C. Liu,^{a,1} M.-Y. Liu,^c X.-L. Qian,^{a,f} Z. Tian,^{a,e} Z. Wang,^{a,e} L. Xue,^d X.-Y. Zhang^d and Xi-Ying Zhang^a

^aKey Laboratory of Particle Astrophysics, Institute of High Energy Physics, Chinese Academy of Sciences, Beijing 100049, China

^bSchool of Nuclear Science and Technology, Lanzhou University, Lanzhou 730000, China

^cPhysics Department of Science School, Tibet University, Lhasa 850000, China

^dShandong University, Jinan 250100, China

^eUniversity of Chinese Academy of Sciences, Beijing 100049, China

^fShandong Management University, Jinan 250100, China

E-mail: liuc@ihep.ac.cn

ABSTRACT: The hybrid Tibet AS array was successfully constructed in 2014. It has 4500 m² underground water Cherenkov pools used as the muon detector (MD) and 789 scintillator detectors covering 36900 m² as the surface array. At 100 TeV, cosmic-ray background events can be rejected by approximately 99.99%, according to the full Monte Carlo (MC) simulation for γ -ray observations. In order to use the muon detector efficiently, we propose to extend the surface array area to 72900 m² by adding 120 scintillator detectors around the current array to increase the effective detection area. A new prototype scintillator detector is developed via optimizing the detector geometry and its optical surface, by selecting the reflective material and adopting dynode readout. This detector can meet our physics requirements with a positional non-uniformity of the output charge within 10% (with reference to the center of the scintillator), time resolution FWHM of ~ 2.2 ns, and dynamic range from 1 to 500 minimum ionization particles.

KEYWORDS: Performance of high-energy physics detectors, Scintillators and light guides, Detector design and construction technologies

¹Corresponding author.

Contents

1	Introduction	1
2	Detector design	2
2.1	Optical surface of the scintillator	3
2.2	Design of the output circuit	4
2.3	Optimization of the detector geometry	4
3	Performance of the prototype detector	6
3.1	Signal of the single particle	7
3.2	Time resolution	7
3.3	Uniformity of the output charge	7
3.4	Linearity	9
4	Summary	10

1 Introduction

Since the discovery of cosmic rays (CRs) in 1912, their origin remains a fundamental problem. Many astrophysical objects, such as supernova remnants (SNRs) [1–3], galactic center (GC) [4–6], and others [7, 8], are supposed to generate expanding diffusive shocks and accelerate CRs to a very high energy. At current status, to observe γ -rays is the optimal way to identify which object makes the dominant contribution. In recent years, great progress in the measurement of the γ -rays have been made with new generation of space borne and ground-based experiments. The Fermi large area telescope (LAT) observed the characteristic pion-decay feature in the γ -ray spectra of three SNRs, IC 443, W44, and W51C [9, 10]. This detection provides direct evidence that CR protons are accelerated in SNRs. Peta-electron volt CRs, likely being accelerated by the GC, recently have been reported by the HESS experiment [11]. Though all these discoveries shed some light on the problem of the CR origin, the dominant sources of the contribution to galactic cosmic rays (GCRs) is still unclear, and it is necessary to discover new hadronic sources. Due to fast energy loss of an electron by synchrotron radiation and inverse Compton scattering with a background photon and the Klein–Nishima effect, a hard γ -ray spectrum in the 100 TeV energy range is believed to originate from the decay of π^0 generated in the interaction of very high-energy CRs with the ambient gas [12]. Therefore, the observation of γ -ray sources in the 100 TeV energy range is one of the best ways to resolve the problem of GCR origin.

With the advantages of both high altitude and wide field of view, the Tibet AS γ experiment was started in 1990 at Yangbajing (90^o31′ E, 30^o06′ N; 4300 m above sea level) in Tibet, China. The Tibet AS experiment currently has the surface array with 789 scintillator detectors covering an

area of 36900 m² and the 4500 m² underground water Cherenkov pools used to select muons[13–15]. The Monte Carlo (MC) simulation predicts that CR background events will be rejected by approximately 99.99% at 100 TeV using this upgraded hybrid experiment [16]. In order to use the muon detector efficiently and to increase the effective detection area, one upgrade is proposed by adding 120 scintillator detectors around the current array. The area of the surface array can be extended to 72900 m² according to this proposal.

Scintillator detectors are widely used in extensive air shower (EAS) experiments (e.g., Tibet AS γ [17], KASCADE-Grande [18], GRAND [19], and so on). For the Tibet AS γ array, scintillator detectors have been running stably for more than 25 years. In the large high-altitude air shower observatory (LHAASO), it is also planned to build 5195 scintillator detectors, each with an area of 1 m², as electromagnetic particle detector (ED) array [20, 21]. This paper introduces the design and performance of the new prototype detector for the Tibet AS surface array.

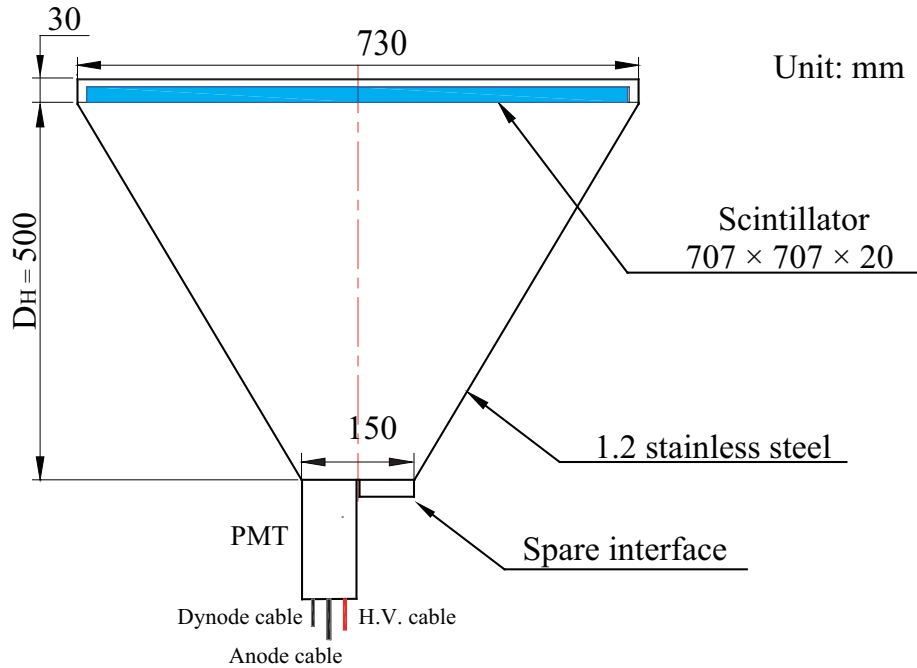


Figure 1. Schematic diagram of the prototype scintillator detector.

2 Detector design

The scintillator detector is easy to be installed and maintained, and it can achieve a long-term stable performance as well as a good time resolution. A new prototype scintillator detector is developed for the proposed upgrading of the Tibet AS array by adopting an air light guide structure. Figure 1 shows the schematic diagram of the designed prototype. The frame structure is made of stainless steel with an upside-down pyramidal shape. The interfaces of the frame are lighttight. The reflective material, DupontTMTyvek[®] 1082D¹, is glued on the inner surface of the frame to

¹<http://www.dupont.com>

increase the efficiency of light collection significantly. An EJ200 plastic scintillator is adopted with a size of 707 mm × 707 mm × 20 mm and placed onto the top of the frame (in Figure 1). A photomultiplier tube (PMT), Hamamatsu R7725, with a diameter of 2 inches is chosen and installed onto the bottom. The detector height (D_H), from the undersurface of the scintillator to the PMT, is set to 500 mm. Next to the PMT, there is a spare interface for further extension and testing. When charged particles pass through the scintillator, photons will be generated. Some of these photons could be refracted into the air light guide, reflected inside the air light guide, and finally collected by the PMT.

2.1 Optical surface of the scintillator

Optical photons are emitted isotropically in the scintillator. A fraction of photons will be entirely reflected when they strike the polished boundary of the scintillator at an angle larger than the critical angle (full reflection angle, θ_c), as shown in the Figure 2-a. To reduce this total reflection effect and to increase the light output, one surface of the scintillator is sanded where the photons will be reflected and diffused in random directions, as demonstrated in figure 2-b.

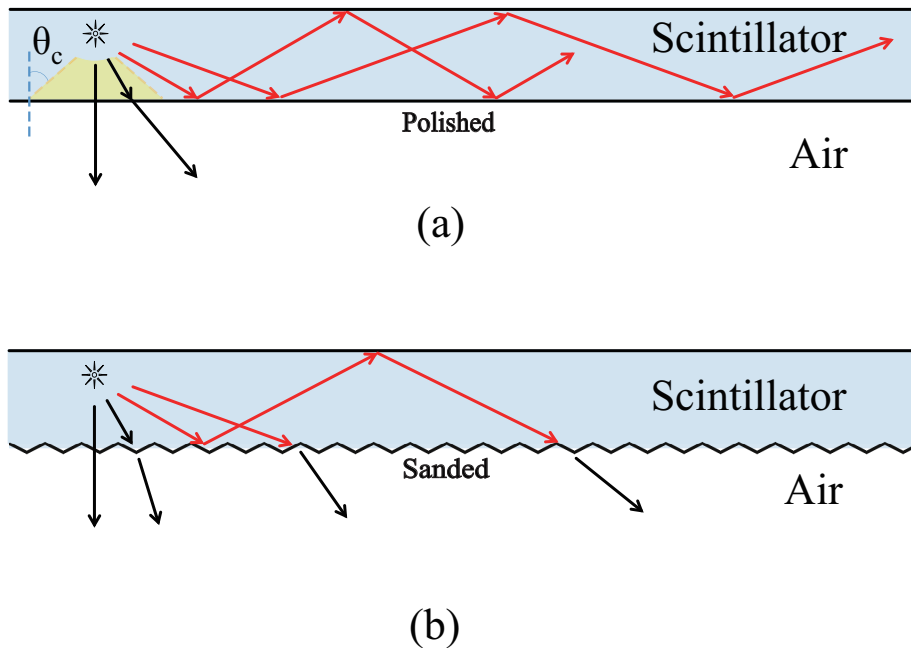


Figure 2. Refraction and total internal reflection of light at the interface between the scintillator and the air light guide. (a) Two polished surfaces; (b) One surface polished and one surface sanded.

In this prototype, the plastic scintillator has one polished surface, one sanded surface, and four machine-cut edges. The undersurface of the scintillator is sanded. The polished surface and four edges of the scintillator are covered with Tyvek 1082D. Compared with the two-polished-surface scintillator, the scintillator with one polished surface and one sanded surface provides an increase in light collection by $\sim 20\%$.

the air can be described by five parameters: specular lobe reflection probability (Csl), specular spike reflection probability (C_{ss}), diffuse lobe reflection probability (Cdl), back scatter reflection probability (Cbs), and σ_α . The values of these parameters are listed in table 1.

Table 1. Parameters used in the Unified Model.

	Csl	C _{ss}	Cdl	Cbs	σ_α
Polished surface	98.9%	0	1.1%	0	0.1
Sanded surface	89%	0	11%	0	0.04
Machine-cut edges	96.7%	0	3.3%	0	0.12

Table 2. Parameters of the scintillator and Tyvek 1082D used in the prototype detector.

Scintillator EJ-200	Parameters
Light output/ % Anthracene	64
Scintillation efficiency/ (photons/MeV)	10000
Wavelength of max. emission/ nm	425
Rise time/ ns	0.9
Decay time/ ns	2.1
Pulse width, FWHM/ ns	2.5
No. of H atoms/ ($10^{22}/cm^3$)	5.17
No. of C atoms/ ($10^{22}/cm^3$)	4.69
No. of electrons/ ($10^{22}/cm^3$)	3.33
Density/ (g/cc)	1.023
Refractive index	1.58
Tyvek 1082D	Parameters
Unit mass/ (g/m^2)	105
Thickness/ μm	275
Opacity/ %	98.4
Longitudinal elongation/ % (N/2.54cm)	290
Transverse elongation/ % (N/2.54cm)	330
Bursting strength/ KPa	1700

When most of the photons come out of the scintillator, they are reflected by high-reflective Tyvek 1082D. The Tyvek 1082D parameters are listed in table 2; its reflectivity was measured at Shandong Metrology Institute in China. After the propagation in the light-guide, only a part of these photons can be collected by the PMT, which is limited by the PMT quantum efficiency (QE) and the photoelectron collection efficiency of the first dynode. In the simulation, the emission spectrum of the scintillator, reflective efficiency of Tyvek 1082D, and quantum efficiency of PMT R7725 [24] are shown in figure 4. Based on the parameters above, the optimization of the frame structure of the light guide is performed.

The frame structure of the detector is an upside-down pyramid shown in Figure 1, so the performance of the detector mainly depends on its area and height. The area of the plastic scintillator plate is fixed at $0.5 m^2$ to keep consistency with the previous one in the Tibet ASy array. In this case,

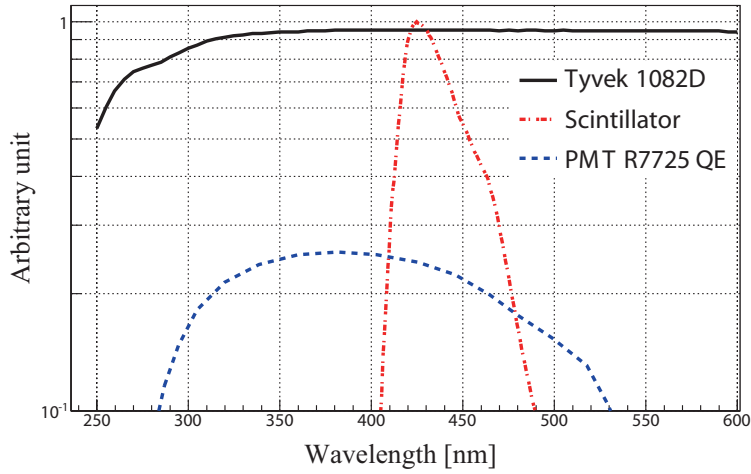


Figure 4. Emission spectrum, quantum efficiency, and Tyvek 1082D reflectivity used in the Optical Model.

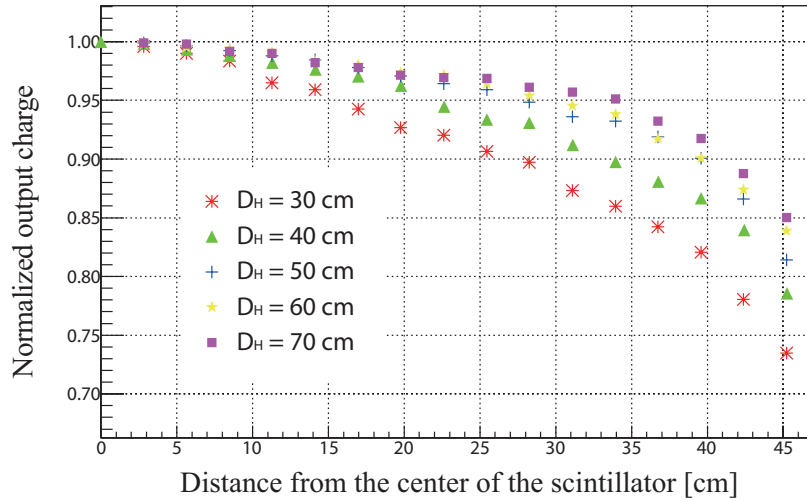


Figure 5. Simulated uniformity (with reference to the center of the scintillator) at different D_H .

the crucial properties of the scintillator detector, such as light collection efficiency, time resolution, and positional uniformity of the output charge, are mainly determined by the height. Figure 5 shows the positional uniformity at different detector heights from the MC simulation. With a height above 50 cm, non-uniformities are less than 20% with reference to the center of the scintillator. In fact, the higher the detector, the better the uniformity is, but the poorer the time resolution and the light output are. Based on this, a detector height of 50 cm is selected for the prototype.

3 Performance of the prototype detector

The properties of the prototype detector, such as single particle response, time resolution, uniformity, and dynamic range, are given as follows.

3.1 Signal of the single particle

When secondary particles produced in an air shower hit the detector and interact with the scintillator, their energy will be deposited and transformed into fluorescent light. These optical photons are then converted to electrons at the photocathode and multiplied by the dynodes of the PMT. Cosmic muons are used to test the detector in our laboratory. The anode output signal is divided into two by a fan-in/out. One goes to the discriminator, and another one goes to the QDC. PMT R7725 works at a high voltage of 1600 V with a gain of $\sim 1 \times 10^7$. The threshold voltage is 30 mV, corresponding to ~ 0.25 MIPs. Figure 6 shows the photoelectron distribution in the self-trigger mode. This distribution can be best fitted by a Landau function (energy deposit of single particles) plus an exponential function (contributions of the noise). The most probable value is ~ 83 photoelectrons.

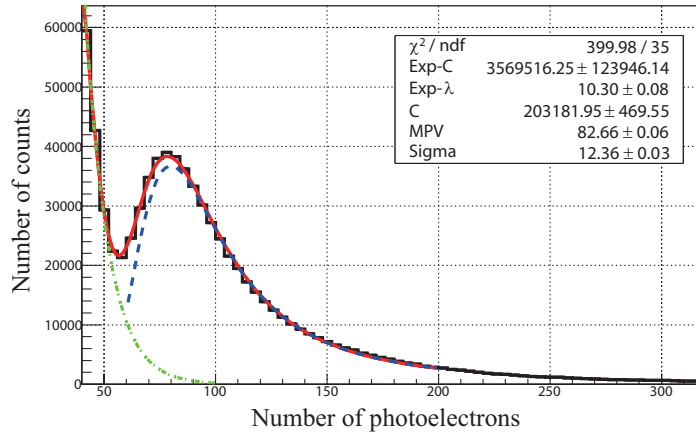


Figure 6. Single-particle distribution of the prototype detector. The fitted plots include detector noise (dashed-dotted line), signal of a single particle (dashed line), and their sum (solid line).

3.2 Time resolution

For the EAS experiment, the direction of a primary CR can be inferred from the relative arrival time of secondary particles hitting the detectors. A high-precision measurement of the arrival time is very important for the direction reconstruction. To measure the time resolution of the prototype detector, a probe scintillator detector ($5 \text{ cm} \times 5 \text{ cm} \times 5 \text{ cm}$) used as a reference was placed on the center of the prototype detector. The time resolution of the probe detector is much better than that of the prototype detector as its PMT is directly coupled to the 5-cm-thick scintillator. Coincidence events between the probe detector and the prototype detector are selected. Figure 7 shows the time resolution FWHM of the prototype detector, which is ~ 2.2 ns.

3.3 Uniformity of the output charge

To study the positional uniformity of the output charge of the detector, the probe detector mentioned in section 3.2 was placed on 7 points along the diagonal (from center position A to edge position G, with a spacing of 5 cm) shown in figure 8-a. Figure 8-b shows the normalized output charge as a function of the position, where one can see that the data (blue squares) and the MC simulations (red triangles) described in section 2.3 are in good agreement. The non-uniformity of the output charge

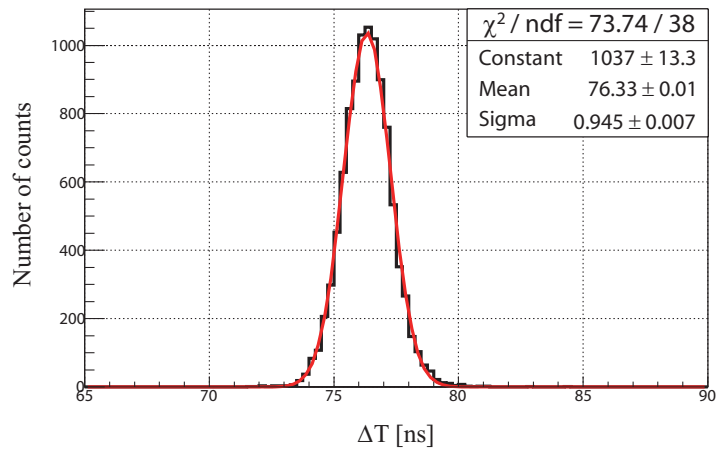


Figure 7. Time resolution of the prototype detector.

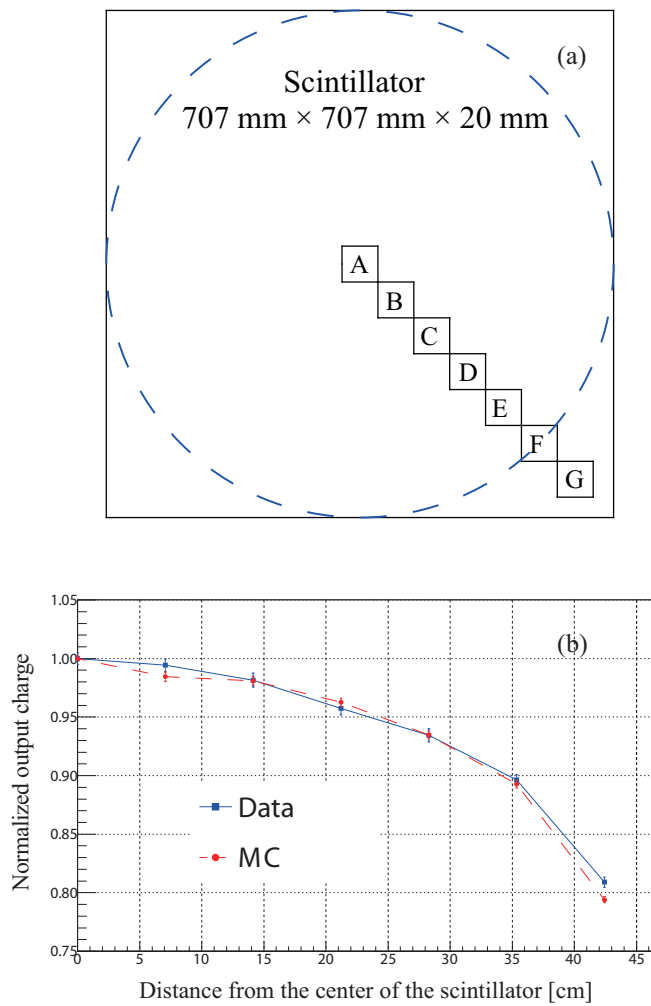


Figure 8. (a) Experimental set-up for the uniformity measurement. (b) Uniformity of the prototype detector (with reference to the center of the scintillator).

(from position A to F) is within 10% with reference to the position A. On the corners (position G), the charge decreases quickly because of the edge effects.

It should be noted that only the main structures and materials are simulated in section 2.3. In the real detector, support structures are added onto four top corners to hold the plastic scintillator. These support structures can affect $\sim 3\%$ the efficiency of the light collection. Nevertheless, the uniformity of the prototype detector could fulfill the requirement of our experiment.

3.4 Linearity

The linearity of the detector mainly depends on the dynamic range of the PMT, because the plastic scintillator could not be saturated below 10^6 MIPs [25]. In this experiment, PMT R7725 has a typical linear current ($\pm 5\%$ nonlinearity) of about 80 mA [24]. To extend its dynamic range, the ninth dynode output is used as the readout to measure the large signal. With the voltage divider circuit shown in figure 3, the dynamic range of the anode output is 1-15 MIPs, while the dynode output covers the dynamic range from 5 to 500 MIPs. The overlap region can be used to calibrate the dynode gain.

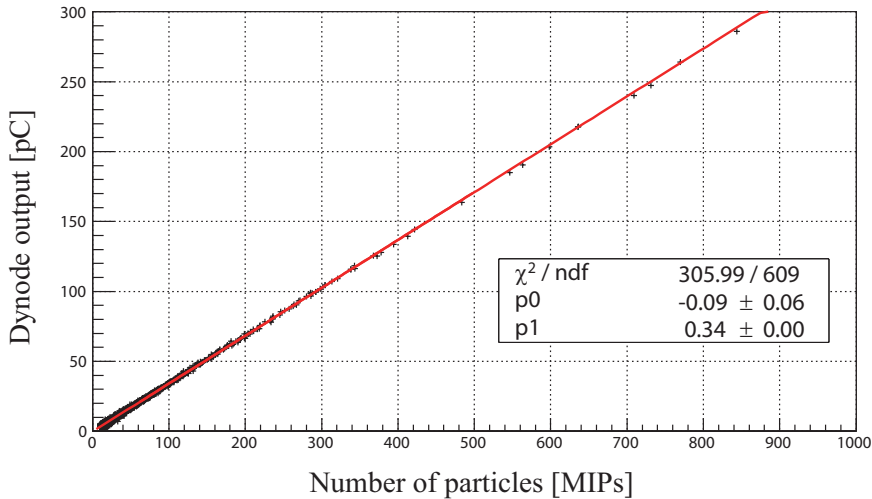


Figure 9. Linearity of the prototype detector.

To test the linearity of the dynode readout, a calibrated PMT ET9829B is installed on the spare interface. The spare and the employed interfaces are symmetrically placed in the frame structure of the detector. Therefore, equal photon numbers could be collected by the two PMTs in statistically. The number of the MIPs can be estimated by the photons collected by the calibrated PMT. ET9829B's linear range could be up to 1000 MIPs, with a working voltage of 1100 V, and PMT R7725 works at a high voltage of 1240 V. Figure 9 shows the dynode output of PMT R7725 as a function of the calibrated PMT's output. This linear relationship indicates that the linearity of prototype detector is good in a range from 1 to 850 MIPs.

4 Summary

A new air light-guide scintillator detector, with a good time resolution, moderate uniformity and dynamic range, is designed and developed to increase the effective detection area of the Tibet AS γ array. The optimization of the detector geometry, scintillator surfaces, reflective material, and readout system was carried out. The test experiment showed that the detector's time resolution FWHM is ~ 2.2 ns and positional non-uniformity of the output charge within 10% (with reference to the center of the scintillator). By using dynode readout, we can obtain the required dynamic range from 1 to 500 MIPs with one PMT.

Acknowledgments

This work is supported by Natural Science Foundation of China (11135010, 11165013, 11375209, 11405180, 11405182, 11563007, 11635011, 11663006, 11775233), 973 Program of China (2013 CB837000), Youth Innovation Promotion Association, Chinese Academy of Sciences, Natural Science Foundation of Tibet Autonomous Region (2016ZR-TU-12), Youth Development Foundation of Tibet University (ZDPJZK1509). We thank the editor and anonymous referees for several valuable suggestions and comments, which have greatly helped to improve the paper.

References

- [1] Bell A. R., The acceleration of cosmic rays in shock fronts. I, *Monthly Notices of the Royal Astronomical Society*, 1978, 182, 147-156
- [2] Bell A. R., The acceleration of cosmic rays in shock fronts. II, *Monthly Notices of the Royal Astronomical Society*, 1978, 182, 443-455
- [3] Blandford, R. D. and Ostriker, J. P., Particle acceleration by astrophysical shocks, *The Astrophysical Journal*, 1978, 221, 29-32
- [4] Ptuskin, V. S. and Khazan, Y. M., The galactic center and the origin of cosmic rays, *Sov. Astron.*, 1981, 25(5), 959-968
- [5] Guo, Y.-Q. et al., On the Galactic Center being the main source of galactic cosmic rays as evidenced by recent cosmic ray and gamma ray observations, *New Journal of Physics*, 2013, 15, 013053
- [6] Guo, Y.-Q. et al., The Galactic Center: A Petaelectronvolt Cosmic-ray Acceleration Factory, *The Astrophysical Journal*, 2017, 836, 233-237
- [7] Waxman, E., Cosmological Gamma-Ray Bursts and the Highest Energy Cosmic Rays, 1995, *Physical Review Letters*, 75, 386:389
- [8] Henri, G., Pelletier, G., Petrucci, P. O. & Renaud, N., Active galactic nuclei as high energy engines, 1999, *Astroparticle Physics*, 11, 347:356
- [9] Ackermann, M. et al., Detection of the Characteristic Pion-Decay Signature in Supernova Remnants, *Science*, 2013, 339, 807-811
- [10] Jogler, T. and Funk, S., Revealing W51C as a Cosmic-Ray source using Fermi-LAT data, *The Astrophysical Journal*, 2016, 816, 100
- [11] Abramowski, A. et al., Acceleration of petaelectronvolt protons in the Galactic Centre, *Nature*, 2016, 531, 476-479

- [12] Atoyan, A. M. et al., Electrons and positrons in the galactic cosmic rays, *Physical Review D Particles & Fields*, 1995, 52, 3265-3275
- [13] Amenomori, M. et al., The TIBET AS+MD Project; progress report 2015, 34th ICRC, 2015, GA, 0969
- [14] Zhaoyang Feng, et al., Study on the Separation of 100 TeV γ -rays from Cosmic Rays with Tibet AS γ Experiment, *Chinese Physics C (HEP & NP)*, 2011, 35(2): 153-157
- [15] Cheng Liu, et al., Performance of the muon detector A under TIBET III array, *Chinese Physics C*, 2013, 37(2), 026001
- [16] The Tibet AS γ Collaboration, The TIBET AS+MD Project; progress report 2011, 32nd ICRC, 2011, OG1.5, 0351
- [17] Amenomori, M. et al., Tibet Air Shower Array: Results and Future Plan, *Journal of Physics: Conference Series*, 2008, 120, 062024
- [18] Antoni, T., et al., The cosmic-ray experiment KASCADE, *Nucl. Instrum. Methods Phys. Res. A*, 2003, 513, 490
- [19] Quanbu Gou, et al., R&D of EAS radio detection in China, 34th ICRC, 2015, CR, 0632
- [20] Zhen Cao, A future project at tibet: the large high altitude air shower observatory, *Chinese Physics C (HEP & NP)*, 2010, 34(2): 4, 249-252
- [21] Ye Liu, et al., Expectation on Observation of Supernova Remnants with the LHAASO Project, *The Astrophysical Journal*, 2016, 826, 63-70
- [22] http://www.eljentechnology.com/images/products/data_sheets/EJ-200_EJ-204_EJ-208_EJ-212.pdf
- [23] Levin, A. and Moisan, C., A more physical approach to model the surface treatment of scintillation counters and its implementation into DETECT, *IEEE Nucl. Sci. Symp. Conf. Rec.* 2(1996) 702
- [24] http://www.hamamatsu.com/resources/pdf/etd/R7723_R7724_R7725_TPMH1315E.pdf
- [25] Amenomori, M. et al., Calibration of the Yangbajing air-shower core detector (YAC) using the beam of BEPC, in the proceedings of the 32nd International Cosmic Ray Conference (ICRC2011), August 11-18, Beijing, China (2011).